Nano Research
2021, 14(1): 239–244
ISSN 1998-0124 CN 11-5974/O4
https://doi.org/10.1007/s12274-020-3075-3

Research Article

Breakdown of Raman selection rules by Fröhlich interaction in few-layer WS_2

Qing-Hai Tan[1], Yu-Jia Sun[1], Xue-Lu Liu[1], Kai-Xuan Xu[1], Yuan-Fei Gao[1,2], Shu-Liang Ren[1], Ping-Heng Tan[1,2], and Jun Zhang[1,2] (✉)

[1] *State Key Laboratory of Superlattices and Microstructures, Institute of Semiconductors, Center of Materials Science and Optoelectronics Engineering, CAS Center of Excellence in Topological Quantum Computation, University of Chinese Academy of Sciences, Beijing 100083, China*

[2] *Beijing Academy of Quantum Information Science, Beijing 100193, China*

Received: 6 July 2020 / **Revised:** 16 August 2020 / **Accepted:** 20 August 2020

ABSTRACT

The polarization selection rule of Raman scattering is crucial in symmetry analysis of elementary excitations in semiconductors and correlated electron systems. Here we reported the observation of breakdown of Raman selection rules in few-layer WS_2 by using resonant Raman spectroscopy. When the excitation energy is close to the dark A exciton state, we observed some infrared active modes and backscattering forbidden modes. Importantly, we found that all observed phonon modes follow the same paralleled-polarization behavior. According to the electron-phonon coupling near the band edge in WS_2, we proposed a theoretical model based on the intraband Fröhlich interaction. In this case, the polarization response of the scattering signal is no longer determined by the original Raman tensor of scattered phonons. Instead, it is determined by a new isotropic Raman tensor that generated from this intraband Fröhlich interaction between dark A exciton and phonons. We found that this theoretical model is in excellent agreement with the observed results. The breakdown of Raman selection rules can violate the conventional limitations of the optical response and provide an effective method to control the polarization of Raman scattering signals in two-dimensional materials.

KEYWORDS

WS_2, resonant Raman scattering, dark exciton, Raman section rules, Fröhlich interaction

1 Introduction

As a fast and non-destructive tool, Raman scattering plays important roles in fundamental research such as the symmetry analysis of crystal materials [1], the electron-phonon coupling (EPC) [2, 3], polaritons in semiconductors [4, 5], and electronic excitation in superconductors [6, 7]. Generally, the Raman scattering processes must follow the so-called Raman selection rules, which are governed by the Raman tensor of the scattered phonons [1]. Specifically, through the Raman selection rules, we can classify the phonon modes as Raman-active or infrared (IR)-active based on the parity of phonons. Besides the activity of phonon modes, the polarization Raman selection rules provide rich information on the symmetric and anisotropic features of lattice vibration and other element excitations [7]. For example, the strong polarization response of the scattering signal has helped build spectroscopic criteria on the gap anisotropy of $YBa_2Cu_3O_7$ superconductor [6], and lasing action of Raman laser [8]. Several reports found that the Raman selection rules can be broken by the local electric field gradient (EFG) effects [9, 10] in metal plasmonic structure contacted carbon nanotubes [11, 12], and the strong EPC effects in Cu_2O and CdS semiconductors [13, 14]. The reduced restriction of optical transitions from the selection rules under these cases is expected to provide the significant advantage of improving the efficiency and diversity of light-matter interaction [12, 13]. In contrast to the EPC dominated resonant Raman scattering, additional conditions such as a special plasmonic substrate are required in the EFG Raman scattering. It is therefore of fundamental significance to explore the EPC effects on the Raman selection rules.

The rise of two-dimensional (2D) materials and their van der Waals (vdW) heterostructures provide a promising platform for fundamental research and optoelectronic device applications [15, 16]. Transition metal dichalcogenides (TMDs) as one of the outstanding representatives due to they have strong spin-orbit coupling (SOC) and interact strongly with light [17, 18]. The strong SOC splits their valance band and conduction band at K point and results in the bright A, B exciton, and dark A, B exciton with different symmetry [19, 20], respectively. The multiple exciton states nature of TMDs is suitable to study the strong EPC induced intriguing phonon physics. For instance, the greatly enhanced intensity of phonon modes in few-layer TMDs and WS_2/hBN heterostructures [21–24], the activated acoustic and IR phonon modes in WS_2 [25], and the improved valley polarization by suppressing the EPC in monolayer MoS_2 [26]. In addition, the polarization response of Raman signal provides an effective method to identify the vibration way of phonon modes [24, 27, 28] and determine the crystal orientation of anisotropy 2D materials such as BP and ReS_2 [29–31], and

Address correspondence to zhangjwill@semi.ac.cn

also opens a door to study the quantum entanglement between phonons and single-photons in monolayer WSe_2 [32]. Particularly, in these polar TMDs semiconductors, the EPC near the band edge is dominated by the intraband Fröhlich interaction [14, 33]. Therefore, it would be very interesting to study the polarization response of the scattering signal with strong EPC in TMDs. However, most of these studies focused on activating forbidden modes or enhancing Raman signal, but how the strong EPC affects the polarization Raman selection rules in such TMDs materials remains unknown.

Here we reported an abnormal polarization Raman behavior in a few-layer WS_2 under resonant excitation. By using multiple linearly polarized lasers, we found the polarization Raman selection rule is broken when the excitation energy is resonant with dark A state. Under this case, the polarization of all Raman modes becomes parallel polarization and independent on the Raman tensors of involved phonons. We attribute this breakdown of Raman selection rules to the intraband Fröhlich interaction between the isotropic s-state of dark A exciton and scattered phonons.

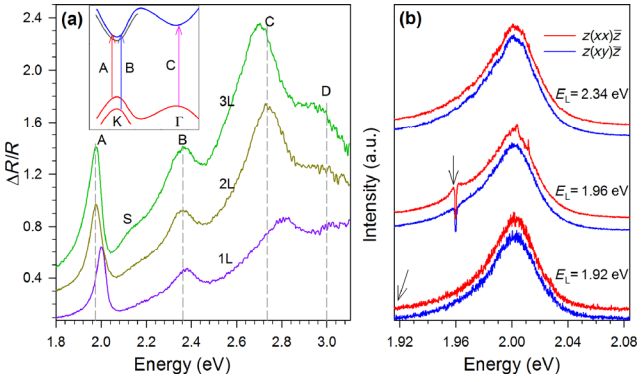

Figure 1 (a) Reflectance contrast spectra $\Delta R/R$ of 1L, 2L, and 3L WS_2 crystals on SiO_2/Si substrate at room temperature. The inset is a schematic of the transition of bright A, B, and C exciton. The dark state (the gray line) is slightly below the bright state. (b) The polarized PL spectra of bright A exciton from 1L WS_2. The excitation energies are close to B, and A exciton states, which corresponds to downconversion and upconversion excitation process, respectively. The arrow shows the energy position of the excitation laser.

2 Experimental

The samples were prepared from bulk WS_2 crystals onto SiO_2/Si substrate by using the micromechanical exfoliation technique. Raman measurements were undertaken in back-scattering geometry with a Jobin-Yvon HR800 system equipped with a liquid-nitrogen-cooled charge-coupled detector. The spectra were collected with a 100× objective lens (NA = 0.9) and 1,800 lines·mm^{-1} grating. The excitation laser (E_L) lines of 457 and 488 nm are from an Ar^+ laser; the laser lines of 612 and 633 nm are from a He-Ne laser; the laser lines of 530, 647 and 676 nm are from a Kr^+ laser. The ultralow-frequency Raman spectra were obtained down to ±5 cm^{-1} by combining three-volume Bragg grating filters into the Raman system to suppress the Rayleigh signal efficiently. To avoid the laser heating to the samples, we kept the laser power below a maximum of 0.2 mW. The reflectance contrast $\Delta R/R$ were undertaken with a 100× objective lens (NA = 0.9) and a 100 lines·mm^{-1} grating with white light. All optical measurements are performed at room temperature.

3 Results and discussion

3.1 Results

Figure 1(a) shows the reflectance contrast spectra $\Delta R / R$ of the monolayer to trilayer (1L–3L) WS_2 at room temperature. Two features at around 1.98 eV (627 nm) and 2.35 eV (528 nm) are denoted by bright A and bright B exciton, which originates from the direct transitions between the spin-orbit split valence band and the conduction at K (or K′) point of the Brillouin zone [34], respectively, as shown in the inset in Fig. 1(a). The C peak at around 2.7 eV (460 nm) is from the transition between the highest valence band and the lowest conduction bands around the Γ point of the Brillouin zone [35], as shown in the inset in Fig. 1(a). The peak at around 2.15 eV (576 nm) denoted by S may correspond to the excitonic Rydberg states of A exciton [36]. The origin of D peak at around 413 nm (3.0 eV) is not clear so far. Owing to the direct bandgap of the 1L-WS_2, the energies of A, B, and C excitons in 1L are slightly larger than those in the bilayer (2L) and trilayer (3L) WS_2, as shown in Fig. 1(a). The energies of A and B excitons are almost the same for 2L and 3L-WS_2, implying they should have similar resonant Raman behavior. The energy differences between bright A and bright B exciton in the 2L- and 3L-WS_2 are slightly large than that in 1L-WS_2, indicating that the spin-orbit coupling strength in bilayer or more layers is stronger than that in 1L-WS_2. Moreover, in contrast to the bright A and B excitons, C exciton is much less confined to a single layer WS_2 [21, 37]. Figure 1(b) shows the polarized photoluminescence (PL) spectra of bright A exciton (X_0) of 1L-WS_2 with three different excitation lasers, where one is downconversion PL excited by 2.34 eV (530 nm), another two are upconversion PL excited by 1.96 eV (633 nm) and 1.92 eV (647 nm), respectively. The intensities of X_0 peaks are almost the same under parallel $(z(xy)\bar{z})$ and cross $(z(xy)\bar{z})$ polarization configurations, implying the bright A exciton is isotropic. As a result, the emission and absorption of bright A excitons are depolarized for linearly polarized laser at room temperature. The observed upconversion PL in monolayer WS_2 suggests that the phonons and EPC play an important role in forming the A excitons. Besides the bright excitons, a small splitting of conduction band results in the dark A and B exciton [19, 20]. Generally, these dark states are laid below the bright states for WX_2 (X = S, Se) (as shown in the inset in Fig. 1(a)), while they are reversed for MoX_2 [19, 20]. The PL spectra of dark A exciton from WX_2 has been directly observed by different experiment methods [38–41].

To study the polarization behaviors of Raman scattering signal under resonant excitations, we performed the polarized Raman measurements with different excitation wavelengths, as shown in Fig. 2. Because the PL signal background of monolayer WS_2 is too strong to identify a good Raman signal when the excitation energies are close to A exciton (as shown in Fig. 1(b)), and the interlayer shear (S) and interlayer breathing (LB) modes is absent in the monolayer case, we only measured the Raman spectra of 2L–4L WS_2. In addition, both the infrared (IR) active S and LB modes can be found in the trilayer case but they are absent in the bilayer case, here we presented the Raman results of 3L-WS_2 in the main text. More experimental results of 2L- and 4L-WS_2 can be found in the Electronic Supplementary Material (ESM). The intensity of Raman mode can be described as: $I \propto \left|\mathbf{e}_s \cdot \mathcal{R} \cdot \mathbf{e}_i\right|$, where $\mathcal{R}$ is the Raman tensor of the vibration mode, $\mathbf{e}_i$ and $\mathbf{e}_s$ are the polarization vectors of the incident and scattered photons, respectively. Considering the backscattering configurations, $\mathbf{e}_i(\mathbf{e}_s)$ can only be along x- or y-direction, the corresponded matrix representations are (1,0,0) and (0,1,0), respectively. The polarization behavior of WS_2 Raman modes is determined by their Raman tensors. The detailed descriptions of Raman tensors of all modes in WS_2 are presented

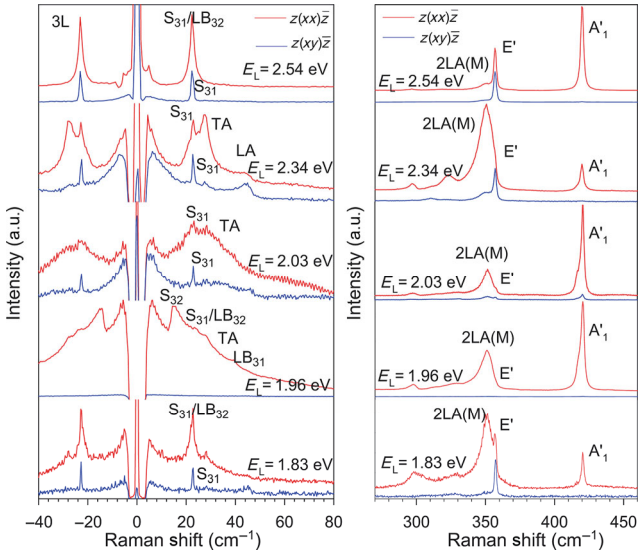

Figure 2 The polarized Raman spectra of 3L-WS_2 with different excitation energies. The left and the right part shows the ultralow and high-frequency region, respectively. Under normal resonant excitation conditions, the in-plane E_{2g}/E' modes both survived at parallel and cross polarization configurations. When the excitation energies are slightly below the bright A exciton state (i.e., close to dark A exciton state), e.g., 1.96 eV, all Raman modes vanished at cross polarized configuration.

in the ESM. Figure 2 shows the Raman spectra of 3L WS_2 under parallel ($z(xx)\bar{z}$) and cross ($z(xy)\bar{z}$) polarization configurations, where the excitation energies are close to C, B, and A exciton, respectively. Under resonance with B or C exciton energies, both the in-plane interlayer S mode and intralayer E′ mode survived under parallel- and cross-polarization configurations, whereas out-of-plane LB mode and intralayer A'_1 mode only survived under parallel configurations, which are consistent with the Raman tensor of these modes. We should note that the frequencies of S_{31} and LB_{32} are close to each other (The fitting result can be found in Fig. S2 in the ESM). In addition, the LA(M) (177 cm^{-1}) and LA(M)+TA(M) (311 cm^{-1}) [42] modes are also observed under both parallel and cross-polarization configurations, see Figs. S1–S3 in the ESM. It indicates these two modes are not polarized under resonant with B or C exciton energies. Remarkably, when the excitation energies are close to the bright A exciton energy (around 1.98 eV), some abnormal phenomena were observed. Specifically, when the excitation energies are slightly higher than or far below than the bright A exciton energy, for example, 612 nm (2.03 eV) and 676 nm (1.83 eV), these modes still comply with the usual Raman selection rules, similar to the case where the excitation energy is resonant with C and B excitons. However, when the excitation energies are slightly below the bright A exciton energy, such as the excitation wavelengths are 633 nm (1.96 eV) and 647 nm (1.92 eV) (also see Figs. S4 and S5 in the ESM), besides the Raman active modes, both the IR-active (e.g., LB_{31}) and normally backscattering forbidden modes (e.g., S_{32}) can be observed with very strong intensity. Interestingly, the in-plane S modes (S_{32} and S_{31}) show an asymmetric Fano line-shape. Remarkably, all of the Raman modes show a strong intensity under parallel polarization configurations but disappear under cross-polarization configurations, including LA(M), and in-plane vibration S_{31} and E' modes. More similar results under this resonance condition can be found in Figs. S4 and S5 in the ESM. The activated forbidden phonon modes can be well explained by considering the parity selection rules are changed when the resonant Raman process involved with dark A exciton [25]. Meanwhile, the Fano lineshape of S modes can be understood through the quantum interference between continuum dark A states and discrete phonon states [25]. The observation of abnormal polarization behaviors indicates that the Raman selection rules were broken under special resonance conditions.

To further study and confirm this abnormal Raman polarization behavior, we measured the polarization resolved Raman spectra of 3L-WS_2 excited by 2.54 and 1.96 eV, respectively. We changed the polarization of incident laser by using a half-wave plate and fixed the polarization of collected signals at the vertical configuration by using a polarizer. Figures 3(a)–(c) show the angle-dependent polarized Raman spectra of 3L-WS_2 with 488 nm (2.54 eV) excitation. The intensities of S mode and E′ mode are independent of the polarization of incident light, whereas the intensity of A'_1 mode shows an angle-dependent behavior. The evolution of the intensity of A'_1 mode with polarization angle can be described by $I \propto \cos^2(\beta)$, where β is

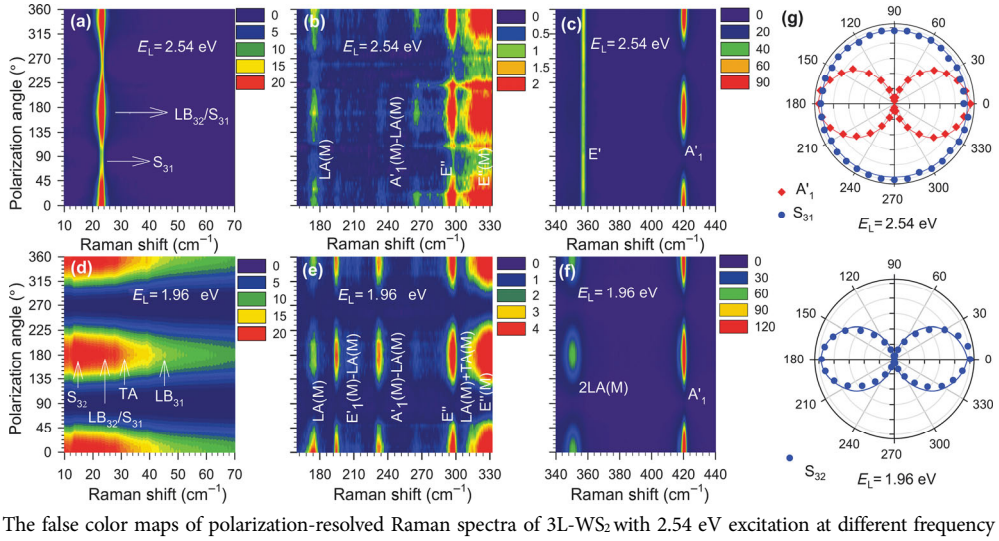

Figure 3 (a)–(c) The false color maps of polarization-resolved Raman spectra of 3L-WS_2 with 2.54 eV excitation at different frequency ranges respectively. (d)–(f) The false color maps of polarization-resolved Raman spectra of 3L-WS_2 with 1.96 eV excitation at different frequency ranges respectively. To clearly see the evolution of Raman intensities with polarization angle, the data is presented in three seperate figures with different frequency ranges. (g) The normalized intensity of A'_1, S_{31}, and S_{32} mode as a function of polarization angle. The upper part is under 2.54 eV and the bottom part is under 1.96 eV excitation. The polarization angle β = 0° (180°) correspondes to parallel polarization configurations, and β = 90° (270°) corresponds to cross polarization configurations.

the polarization angle of excitation laser away from the *y*-axis. Figures 3(d)–3(f) show the angle-dependent polarized Raman spectra of 3L-WS_2 with 633 nm (1.96 eV) excitation. We should note that the energy of this excitation wavelength is close to the energy of dark A exciton. Interestingly, in this case, all modes show the same angle-dependent behavior, including in-plane vibration S modes, TA mode, LA(M) mode, 2LA(M) and A_1' modes. Their intensities also can be described by $I \propto \cos^2(\beta)$. Figure 3(g) shows the polar maps of normalized intensity and polarization angle. Under excited by 2.54 eV, in contrast to the intensities of in-plane S_{31}/E′ modes almost constant with the polarization angle, the intensities of these out-of-plane LB and A_1' modes depend on the polarization angles. Remarkably, when excited by 1.96 eV, all Raman modes show the same polarization-dependent behavior. Similar results of 2L-WS_2 can be found in Fig. S6 in the ESM. These results indicate that under 1.96 eV resonant excitation condition, the polarization behavior of all Raman modes in WS_2 does not obey its original Raman tensors.

3.2 Discussion

We noted that the observation of forbidden Raman modes and abnormal polarization behavior of Raman modes only when resonance with dark A exciton rather than dark B exciton and bright A exciton. This result can be understood that the dark A state is a slightly mixed state with bright A exciton. Consequently, the oscillator strength of dark A exciton is quite small but not equal to zero, while the oscillator strength of dark B is strictly equal to zero [20, 43]. On the other hand, the electrons in bright A exciton state will extremely quickly transit to the lower dark A state by intravalley spin-flip scattering or spin-preserving intervalley scattering process with a much faster time scale than radiative recombination, resulting in the low PL quantum yield of monolayer MX_2 [44, 45]. In particular, the dark A exciton has a longer radiative lifetime, i.e., two orders of magnitude longer than the radiative lifetime of the bright exciton [46]. Consequently, these characteristics will accumulate most electrons in the dark A exciton state to form a continuum state [25, 36]. Therefore, exciton intraband scattering is dominated by the dark state band rather than by the bright state band.

To understand the abnormal polarization behavior of Raman signal in WS_2 under this resonant condition, we need to analyze it from the first-order Raman scattering cross section [14, 33, 47]

$$\sigma = \sigma_0 \frac{\omega_s}{\omega_i}\left|\sum_{\alpha\beta}\mathbf{e}_s^{\alpha}\mathcal{R}^{\alpha\beta}\mathbf{e}_i^{\beta}\right|^2$$

$$\mathcal{R}^{\alpha\beta} = \sum_{ij}\frac{P_{0j}^{\alpha}M_{ij}P_{i0}^{\beta}}{\left(E_j-\omega_i+\omega_0\right)\left(E_i-\omega_s\right)} \quad (1)$$

where σ_0 is the free-electron Compton cross section $(e^2/mc^2)^2$ and α and β are Cartesian indices, $\omega_{s(i)}$ denotes the frequency of scattered (incident) photons, and E_i and E_j denote the energies of excited electronic states, P_{0i}^{α} and P_{0j}^{β} are the momentum matrix element with the ground state 0, M_{ij} is the phonon scattering matrix element, which both the exciton-phonon interaction and exciton-photon interaction are included, ω_0 is the phonon frequency, and $\mathbf{e}_i$ and $\mathbf{e}_s$ are incident and scattered photon polarization. Because the tensorial character of $\mathcal{R}$ determines the polarization selection rules, so we need to consider the expression of $\mathcal{R}$ under resonant condition. The exciton-phonon interactions near the dark A exciton here can be described by considering the intraband Fröhlich interaction [14, 33]. The Hamiltonian $\mathbf{H}(F,q)$ of Fröhlich interaction can be written as [48]

$$\mathbf{H}(F,q) = iC_F/q\left[e^{(ip_h\mathbf{q}\cdot\mathbf{r})} - e^{(ip_e\mathbf{q}\cdot\mathbf{r})}\right]\left(a_{k+q}^{+}a_k\right)\left(C_{-q}^{+}+C_q\right) \quad (2)$$

where $C_F = e\left[\frac{2\pi\hbar\omega_0}{NV}\left(\varepsilon_\infty^{-1}-\varepsilon_0^{-1}\right)\right]^{1/2}\left(4\pi\varepsilon_0\right)^{-1/2}$ is a constant coupling coefficient, N and V are the number of unit cells per unit volume of the crystal and the volume of the primitive cell, respectively. $\boldsymbol{q} = \boldsymbol{k}_i - \boldsymbol{k}_s$ is the wave vector of phonon, and ε_0 is the low-frequency optical dielectric constant and ε_∞ is the static dielectric constant. C_q^{+} and $C_q\left(a_k^{+}\text{ and }a_k\right)$ correspond to the creation and annihilation operators for phonons (excitons), respectively. The r is a characteristic length of the excited state. Since the intraband Fröhlich interaction here connects the s states of dark A exciton, the magnitude of the phonon scattering can be simply written as [47]

$$M_{ij} = \left|\left\langle 1s\left|\mathbf{H}_{(F,q)}\right|1s\right\rangle\right| = \left(\frac{C_F}{q}\right)\left[\left(\frac{1}{1+\left(p_hqr/2\right)^2}\right)^2 - \left(\frac{1}{1+\left(p_eqr/2\right)^2}\right)^2\right] \quad (3)$$

Where $p_e = \frac{m_e}{m_e+m_h}$, $p_h = \frac{m_h}{m_e+m_h}$. For the small but non-negligible q, this magnitude expression can be expanded as

$$M_{ij} \simeq C_F qr\frac{m_e-m_h}{m_e+m_h} \quad (4)$$

Since M_{ij} is a constant only for $i=j$ and is zero for $i\neq j$, the original Raman tensor $\mathcal{R}$ in Eq. (1) degenerates into a scalar quantity: $\mathcal{R}\propto qr$. This result means that the Raman selection rules here are no longer restricted by its original Raman tensors. In contrast, the Raman tensor here becomes isotropic, similar to the s-state of A exciton (more details are present in the ESM). In this case, if we changed the polarization of incident photon and fixed the polarization of collected signals, i.e., $\mathbf{e}_i$ and $\mathbf{e}_s$ are [sinβ, cosβ, 0] and [0, 1, 0], respectively, then the Raman intensity can be simply written as

$$I \propto (qr)^2\cos^2\beta \quad (5)$$

It means the intensity of phonon modes is contributed only by the diagonal scattering and irrespective of its original Raman tensor. Consequently, the intensity of Raman modes reaches the strongest when $\mathbf{e}_i \| \mathbf{e}_s$, and becomes zero when $\mathbf{e}_i \perp \mathbf{e}_s$. The above polarization-dependent experimental results thus, can be fully explained by considering this intraband Fröhlich interaction between dark A exciton and phonons. Because the Raman selection rule under such resonant excitation is independent of the symmetry of crystal. As a result, similar results are expected to be observed in other 2D materials and vdW heterostructures.

4 Conclusions

In summary, we studied the breakdown of polarization Raman selection rules in few-layer WS_2 by resonant Raman spectroscopy. When the excitation energy is close to the dark A exciton state, we observed some IR-active and backscattering forbidden phonon modes. In particular, we found that all Raman modes show the same paralleled-polarization behavior, regardless of its original Raman tensors. Based on the intraband Fröhlich interaction between dark A exciton and phonons, we proposed a model and found it is in excellent agreement with the

experimental results. The present confirmation of breakdown of the selection rules shows the EPC effect not only enhances the intensity of the scattering signal, but also increases the optical excitation channels beyond the selection rules. These characteristic features are expected to provide an effective method to improve the efficiency of light scattering and control the polarization of the scattering signal.

Competing interests: The authors declare no competing financial interest.

Acknowledgements

J. Z. and P. T. acknowledge support from the National Basic Research Program of China (Nos. 2017YFA0303401 and 2016YFA0301200), Beijing Natural Science Foundation (No. JQ18014), and the Strategic Priority Research Program of the Chinese Academy of Sciences (No. XDB28000000).

Electronic Supplementary Material: Supplementary material (the Raman tensors of first-order Raman active phonon modes, Raman spectra of 2-4L WS_2 with different excitation wavelengths, the Feynman diagrams of resonant process, the detailed derivation of EPC effects on Raman tensor) is available in the online version of this article at https://doi.org/10.1007/s12274-020-3075-3.

References

[1] Loudon, R. The Raman effect in crystals. *Adv. Phys.* **1964**, *13*, 423–482.

[2] Huang, K.; Rhys, A. Theory of light absorption and non-radiative transitions in F-centres. *Proc. Roy. Soc. A Mathem., Phys. Eng. Sci.* **1950**, *204*, 406–423.

[3] Zhang, Q.; Zhang, J.; Utama, M. I. B.; Peng, B.; de la Mata, M.; Arbiol, J.; Xiong, Q. H. Exciton-phonon coupling in individual ZnTe nanorods studied by resonant Raman spectroscopy. *Phys. Rev. B* **2012**, *85*, 085418.

[4] Henry, C. H.; Hopfield, J. J. Raman scattering by polaritons. *Phys. Rev. Lett.* **1965**, *15*, 964–966.

[5] Sanvitto, D.; Kéna-Cohen, S. The road towards polaritonic devices. *Nat. Mater.* **2016**, *15*, 1061–1073.

[6] Cooper, S. L.; Slakey, F.; Klein, M. V.; Rice, J. P.; Bukowski, E. D.; Ginsberg, D. M. Gap anisotropy and phonon self-energy effects in single-crystal $YBa_2Cu_3O_{7-\delta}$. *Phys. Rev. B* **1988**, *38*, 11934–11937.

[7] Devereaux, T. P.; Häckl, R. Inelastic light scattering from correlated electrons. *Rev. Mod. Phys.* **2007**, *79*, 175–233.

[8] Shen, X. Q.; Choi, H.; Chen, D. Y.; Zhao, W.; Armani, A. M. Raman laser from an optical resonator with a grafted single-molecule monolayer. *Nat. Photonics* **2019**, *14*, 95–101.

[9] Ayars, E.; Hallen, H. Electric field gradient effects in NSOM-Raman spectroscopy. In *Proceedings of American Physical Society, Annual March Meeting*, Washington, 2001, pp. U96–U96.

[10] Ismail, N.; El-Meligi, A. A.; Temerk, Y. M.; Madian, M. Synthesis and characterization of layered $FePS_3$ for hydrogen uptake. *Int. J. Hyd. Energy* **2010**, *35*, 7827–7834.

[11] Kneipp, K.; Jorio, A.; Kneipp, H.; Brown, S. D. M.; Shafer, K.; Motz, J.; Saito, R.; Dresselhaus, G.; Dresselhaus, M. S. Polarization effects in surface-enhanced resonant Raman scattering of single-wall carbon nanotubes on colloidal silver clusters. *Phys. Rev. B* **2001**, *63*, 081401.

[12] Takase, M.; Ajiki, H.; Mizumoto, Y.; Komeda, K.; Nara, M.; Nabika, H.; Yasuda, S.; Ishihara, H.; Murakoshi, K. Selection-rule breakdown in plasmon-induced electronic excitation of an isolated single-walled carbon nanotube. *Nat. Photonics* **2013**, *7*, 550–554.

[13] Yu, P. Y.; Shen, Y. R.; Petroff, Y.; Falicov, L. M. Resonance Raman scattering at the forbidden yellow exciton in Cu_2O. *Phys. Rev. Lett.* **1973**, *30*, 283–286.

[14] Cardona, M. *Light Scattering in Solids I*: *Introductory Concepts*; Springer: Berlin, Heidelberg, 1983.

[15] Liu, X. L.; Hersam, M. C. 2D materials for quantum information science. *Nat. Rev. Mater.* **2019**, *4*, 669–684.

[16] Liu, Y.; Weiss, N. O.; Duan, X. D.; Cheng, H. C.; Huang, Y.; Duan, X. F. van der Waals heterostructures and devices. *Nat. Rev. Mater.* **2016**, *1*, 16042.

[17] Zeng, H. L.; Cui, X. D. An optical spectroscopic study on two-dimensional group-VI transition metal dichalcogenides. *Chem. Soc. Rev.* **2015**, *44*, 2629–2642.

[18] Wang, G.; Chernikov, A.; Glazov, M. M.; Heinz, T. F.; Marie, X.; Amand, T.; Urbaszek, B. *Colloquium*: Excitons in atomically thin transition metal dichalcogenides. *Rev. Mod. Phys.* **2018**, *90*, 021001.

[19] Dery, H.; Song, Y. Polarization analysis of excitons in monolayer and bilayer transition-metal dichalcogenides. *Phys. Rev. B* **2015**, *92*, 125431.

[20] Echeverry, J. P.; Urbaszek, B.; Amand, T.; Marie, X.; Gerber, I. C. Splitting between bright and dark excitons in transition metal dichalcogenide monolayers. *Phys. Rev. B* **2016**, *93*, 121107.

[21] Scheuschner, N.; Gillen, R.; Staiger, M.; Maultzsch, J. Interlayer resonant Raman modes in few-layer MoS_2. *Phys. Rev. B* **2015**, *91*, 235409.

[22] del Corro, E.; Botello-Méndez, A.; Gillet, Y.; Elias, A. L.; Terrones, H.; Feng, S.; Fantini, C.; Rhodes, D.; Pradhan, N.; Balicas, L. et al. Atypical exciton-phonon interactions in WS_2 and WSe_2 monolayers revealed by resonance Raman spectroscopy. *Nano Lett.* **2016**, *16*, 2363–2368.

[23] Song, Q. J.; Tan, Q. H.; Zhang, X.; Wu, J. B.; Sheng, B. W.; Wan, Y.; Wang, X. Q.; Dai, L.; Tan, P. H. Physical origin of Davydov splitting and resonant Raman spectroscopy of Davydov components in multilayer $MoTe_2$. *Phys. Rev. B* **2016**, *93*, 115409.

[24] Lin, M. L.; Zhou, Y.; Wu, J. B.; Cong, X.; Liu, X. L.; Zhang, J.; Li, H.; Yao, W.; Tan, P. H. Cross-dimensional electron-phonon coupling in van der Waals heterostructures. *Nat. Commun.* **2019**, *10*, 2419.

[25] Tan, Q. H.; Sun, Y. J.; Liu, X. L.; Zhao, Y. Y.; Xiong, Q. H.; Tan, P. H.; Zhang, J. Observation of forbidden phonons, Fano resonance and dark excitons by resonance Raman scattering in few-layer WS_2. *2D Mater.* **2017**, *4*, 031007.

[26] Miller, B.; Lindlau, J.; Bommert, M.; Neumann, A.; Yamaguchi, H.; Holleitner, A.; Högele, A.; Wurstbauer, U. Tuning the Fröhlich exciton-phonon scattering in monolayer MoS_2. *Nat. Commun.* **2019**, *10*, 807.

[27] Liang, L. B.; Zhang, J.; Sumpter, B. G.; Tan, Q. H.; Tan, P. H.; Meunier, V. Low-frequency shear and layer-breathing modes in Raman scattering of two-dimensional materials. *ACS Nano* **2017**, *11*, 11777–11802 .

[28] Zhang, X.; Han, W. P.; Wu, J. B.; Milana, S.; Lu, Y.; Li, Q. Q.; Ferrari, A. C.; Tan, P. H. Raman spectroscopy of shear and layer breathing modes in multilayer MoS_2. *Phys. Rev. B* **2013**, *87*, 115413.

[29] Kim, J.; Lee, J. U.; Lee, J.; Park, H. J.; Lee, Z.; Lee, C.; Cheong, H. Anomalous polarization dependence of Raman scattering and crystallographic orientation of black phosphorus. *Nanoscale* **2015**, *7*, 18708–18715.

[30] Ling, X.; Huang, S. X.; Hasdeo, E. H.; Liang, L. B.; Parkin, W. M.; Tatsumi, Y.; Nugraha, A. R. T.; Puretzky, A. A.; Masih Das, P.; Sumpter, B. G. et al. Anisotropic electron-photon and electron-phonon interactions in black phosphorus. *Nano Lett.* **2016**, *16*, 2260–2267.

[31] Qiao, X. F.; Wu, J. B.; Zhou, L. W.; Qiao, J. S.; Shi, W.; Chen, T.; Zhang, X.; Zhang, J.; Ji, W.; Tan, P. H. Polytypism and unexpected strong interlayer coupling in two-dimensional layered ReS_2. *Nanoscale* **2016**, *8*, 8324–8332.

[32] Chen, X. T.; Lu, X.; Dubey, S.; Yao, Q.; Liu, S.; Wang, X. Z.; Xiong, Q. H.; Zhang, L. F.; Srivastava, A. Entanglement of single-photons and chiral phonons in atomically thin WSe_2. *Nat. Phys.* **2019**, *15*, 221–227.

[33] Martin, R. M. Theory of the one-phonon resonance Raman effect. *Phys. Rev. B* **1971**, *4*, 3676–3685.

[34] Mak, K. F.; Lee, C.; Hone, J.; Shan, J.; Heinz, T. F. Atomically thin MoS_2: A new direct-gap semiconductor. *Phys. Rev. Lett.* **2010**, *105*, 136805.

[35] Qiu, D. Y.; Da Jornada, F. H.; Louie, S. G. Optical spectrum of MoS_2: Many-body effects and diversity of exciton states. *Phys. Rev. Lett.* **2015**, *115*, 216805.

[36] Chernikov, A.; van der Zande, A. M.; Hill, H. M.; Rigosi, A. F.; Velauthapillai, A.; Hone, J.; Heinz, T. F. L. Electrical tuning of exciton binding energies in monolayer WS_2. *Phys*. *Rev*. *Lett*. **2015**, *115*, 126802.

[37] Carvalho, B. R.; Malard, L. M.; Alves, J. M.; Fantini, C.; Pimenta, M. A. Symmetry-dependent exciton-phonon coupling in 2D and bulk MoS_2 observed by resonance Raman scattering. *Phys*. *Rev*. *Lett*. **2015**, *114*, 136403.

[38] Molas, M. R.; Faugeras, C.; Slobodeniuk, A. O.; Nogajewski, K.; Bartos, M.; Basko, D. M.; Potemski, M. Brightening of dark excitons in monolayers of semiconducting transition metal dichalcogenides. *2D Mater*. **2017**, *4*, 021003.

[39] Zhou, Y.; Scuri, G.; Wild, D. S.; High, A. A.; Dibos, A.; Jauregui, L. A.; Shu, C.; De Greve, K.; Pistunova, K.; Joe, A. Y. et al. Probing dark excitons in atomically thin semiconductors via near-field coupling to surface plasmon polaritons. *Nat*. *Nanotechnol*. **2017**, *12*, 856–860.

[40] Wang, G.; Robert, C.; Glazov, M. M.; Cadiz, F.; Courtade, E.; Amand, T.; Lagarde, D.; Taniguchi, T.; Watanabe, K.; Urbaszek, B. et al. In-plane propagation of light in transition metal dichalcogenide monolayers: Optical selection rules. *Phys*. *Rev*. *Lett*. **2017**, *119*, 047401.

[41] Park, K. D.; Jiang, T.; Clark, G.; Xu, X. D.; Raschke, M. B. Radiative control of dark excitons at room temperature by nano-optical antenna-tip purcell effect. *Nat*. *Nanotechnol*. **2017**, *13*, 59–64.

[42] Shi, W.; Lin, M. L.; Tan, Q. H.; Qiao, X. F.; Zhang, J.; Tan, P. H. Raman and photoluminescence spectra of two-dimensional nanocrystallites of monolayer WS_2 and WSe_2. *2D Mater*. **2016**, *3*, 025016.

[43] Zhang, X. X.; Cao, T.; Lu, Z. G.; Lin, Y. C.; Zhang, F.; Wang, Y.; Li, Z. Q.; Hone, J. C.; Robinson, J. A.; Smirnov, D. et al. Magnetic brightening and control of dark excitons in monolayer WSe_2. *Nat*. *Nanotechnol*. **2017**, *12*, pages883–888.

[44] Jin, C. H.; Kim, J.; Wu, K. D.; Chen, B.; Barnard, E. S.; Suh, J.; Shi, Z. W.; Drapcho, S. G.; Wu, J. Q.; Schuck, P. J. et al. On optical dipole moment and radiative recombination lifetime of excitons in WSe_2. *Adv*. *Funct*. *Mater*. **2016**, *27*, 1601741.

[45] Wang, Z. L.; Molina-Sánchez, A.; Altmann, P.; Sangalli, D.; De Fazio, D.; Soavi, G.; Sassi, U.; Bottegoni, F.; Ciccacci, F.; Finazzi, M. et al. Intravalley spin-flip relaxation dynamics in single-layer WS_2. *Nano Lett*. **2018**, *18*, 6882–6891.

[46] Robert, C.; Amand, T.; Cadiz, F.; Lagarde, D.; Courtade, E.; Manca, M.; Taniguchi, T.; Watanabe, K.; Urbaszek, B.; Marie, X. Fine structure and lifetime of dark excitons in transition metal dichalcogenide monolayers. *Phys*. *Rev*. *B* **2017**, *96*, 155423.

[47] Martin, R. M.; Damen, T. C. Breakdown of selection rules in resonance Raman scattering. *Phys*. *Rev*. *Lett*. **1971**, *26*, 86–88.

[48] Yu, P. Y.; Cardona, M. *Fundamentals of Semiconductors*: *Physics and Materials Properties*; 4th ed. Springer: New York, 2010.